

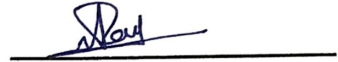
Declaration

I, **Arpita Roy**, hereby declare that the present thesis, entitled “**Fabrication and Characterization of the 2D Tungsten Disulfide (WS₂) Field Effect Transistor**”, is the record of research work done by me under the supervision of Dr. Biplob Mondal, Associate Professor, Department of Electronics and Communication Engineering, Tezpur University, Tezpur. The contents of the thesis represent my original works that have not been previously submitted for any Degree/Diploma/Certificate in any other University or Institutions of Higher Education.

This thesis is being submitted to Tezpur University for the Degree of Doctor of Philosophy in Electronics and Communication Engineering.

Place: Tezpur University, Tezpur

Date: 04/07/2025



(Arpita Roy)





TEZPUR UNIVERSITY

(A Central University Established by an Act of Parliament)

Napaam, Tezpur-784028, Sonitpur, Assam, India

Certificate of the External Examiner

This is to certify that the thesis entitled “**Fabrication and the Characterization of the 2D Tungsten Disulfide (WS₂) Field Effect Transistor**” submitted by **Ms. Arpita Roy** Department of Electronics & Communication Engineering, School of Engineering, Tezpur University in partial fulfilment for the award of the degree of Doctor of Philosophy in Electronics & Communication Engineering has been examined by us on _____ and found to be satisfactory.

The committee recommends for the award of the degree of Doctor of Philosophy.

Supervisor
(Dr. Biplob Mondal)

External Examiner
()

Date: _____

Date: _____

Acknowledgment

Preparing this thesis, entitled “Fabrication and Characterization of the 2D Tungsten Disulfide (WS₂) Field Effect Transistor”, has been one of the most enriching experiences of my academic journey. The knowledge and confidence I gained through this study are invaluable assets that will guide me throughout my career. The successful completion of this thesis would not have been possible without the support, encouragement, and guidance of many individuals to whom I am deeply grateful.

First and foremost, I would like to express my sincere gratitude to my esteemed supervisor, Dr. Biplob Mondal, Associate Professor, Department of Electronics and Communication Engineering, Tezpur University. His expert guidance, continuous support, and insightful advice have been instrumental throughout my research journey. I am especially thankful for the research facilities he provided, which enabled me to carry out my experimental work.

I extend my heartfelt appreciation to the members of my thesis committee, Prof. Partha Pratim Sahu and Dr. Ratul Kumar Baruah, for their valuable insights, constructive critiques, and thoughtful suggestions, which significantly enhanced the quality of my research. I also want to thank all the respected faculty members of my department for their encouragement and for fostering an environment conducive to learning and innovation.

I am sincerely grateful to AICTE for the financial support provided through the AICTE Doctoral Fellowship (ADF) program during my Ph.D., which enabled me to pursue my doctoral studies.

I also appreciate the support from Tezpur University, which provided the necessary resources, research facilities, and a stimulating academic environment. Additionally, I acknowledge the invaluable assistance from the university under the ‘Research and Innovation Grant’ scheme 2021 (Memo No. DoRD/RIG/10-73 1592-A), which facilitated the procurement of essential consumables for my research. I gratefully acknowledge the support received from the DST-FIST project (SR/FST/ET-II/2018/241) of the Department of Science & Technology (DST), Government of India, at the Department of Electronics and Communication Engineering, Tezpur University, for its invaluable contribution to my research work. My heartfelt thanks go to the Sophisticated Analytical Instrumentation Centre (SAIC) and its technical staff, whose expertise and

support in analyzing my research significantly contributed to the success of this thesis. I am also grateful to the lab technicians and staff for their dedication and assistance throughout my experimental work. I extend my sincere gratitude to Assistant Librarian Jitu Moni Das for his invaluable support in conducting a plagiarism check during the initial stages of my thesis submission. His timely assistance ensured adherence to academic integrity standards, contributing significantly to the successful submission of this thesis.

I extend my sincere thanks to the Ministry of Electronics and Information Technology (MeitY), Government of India, for funding this project (No. 5(1)/2021-NANO). I sincerely thank the INUP i2i 2023 program, Centre for Nanotechnology, IIT Guwahati, for supporting my research by accepting my project and providing both funding and technical assistance. Special thanks to Dr. Franco Mayanglambam for his help in booking slots for device fabrication and characterization, which was crucial for the successful completion of my project.

I am deeply thankful to my friends and seniors Aishwarya, Ritayan, Sujay, Aashamoni, Bhupali, Amarprit, Biswajit, Suhriday, Jaharlal, Supriya, Denim, Dimpi, Sita, Dikshita and Suhas D. for their constant support, encouragement, and companionship throughout my Ph.D. journey. I would also like to extend my heartfelt gratitude to my long-time friend Mr. Jagabandhu Mahato, whose encouragement during my PhD admission and unwavering support throughout my career have been invaluable.

I am profoundly grateful to my family, my father, Mr. Harish Chandra Roy, my mother, Mrs. Mamata Roy, and my younger brother, Mr. Puskar Roy for their unwavering love, encouragement, and support. Their steadfast belief in me has been a constant source of strength and inspiration throughout this journey.

Last but not least, I extend my heartfelt gratitude to everyone who has contributed, in ways big or small, to my academic and personal growth, even if their names are not explicitly mentioned here. The successful completion of this thesis would not have been possible without the collective support, encouragement, and guidance of all these individuals and institutions. I am profoundly thankful for their invaluable contributions and unwavering support, which have been a source of strength and inspiration throughout my journey.

Arpita Roy

*Dedicated to my
Parents.....*

List of Figures:

Chapter	Figure	Title	Page No.
1	Fig. 1.1	Evolution of FET structures over time: From traditional Si-based MOSFETs to FinFET and gate-all-around (GAA) transistors, which are expected to dominate the market by the mid-2020s. The evolution continues with the incorporation of 1D and 2D materials like nanotubes and nanosheets, highlighting enhanced scaling and functionality in modern FET designs, and promising further advancements in efficiency and performance.....	3
	Fig. 1.2	Schematic representation of a 1D material-based FET structure: (a) A semiconducting channel composed of a nanotube or nanowire positioned vertically between the source and drain metal contacts, and (b) multiple nanorods arranged horizontally in the FET device, serving as the semiconducting channel between the source and drain metal contacts.....	5
	Fig. 1.3	Illustrates the atomic structures of 2D materials and their corresponding FET structures: (a) graphene (b) Black phosphorus (BP) and (c) Transition Metal Dichalcogenide.....	8
	Fig. 1.4	2D-TMD materials are categorized into three distinct types: Metallic, Superconducting, and Semiconducting.....	9
	Fig. 1.5	Diagrammatic representation of various device architectures based on TMD material for various electronics and optoelectronic applications: FET, biosensor, gas sensor, flexible device, memristor and photodetector	10
	Fig. 1.6	Schematic depiction of energy band diagram of (a) graphene and (b) the indirect bandgap of bulk TMD and the direct bandgap of monolayer TMD.....	11
2	Fig. 2.1	Atomic structure of three typical crystal phases of WS ₂ : (a) 1T-phase tetragonal symmetry with octahedral coordination (b) 2H-Phase hexagonal symmetrical structure (c) 3R-Phase rhombohedral symmetrical structure and (d & e) schematic illustration of the density of states for selected transition metal groups, showing the d-orbital splitting for 1T and 2H/3R phase.....	31

	Fig. 2.2	Band structure of 2H-WS ₂ : (a) Indirect bandgap of bilayer WS ₂ (b) Direct bandgap of monolayer WS ₂ (c) band structure of p-type doped WS ₂ and (d) Band structure of n-type doped WS ₂	33
	Fig. 2.3	Schematical illustration of commonly adopted synthesis method for producing 2D materials: (a) Mechanical exfoliation using scotch tape to extract layers from bulk WS ₂ (b) Liquid-phase exfoliation, producing layered nanosheets from bulk WS ₂ powder through sonication in a suitable solvent (c) Experimental setup illustrating the Vapour phase deposition technique: thermal evaporation of WO ₃ powder and chalcogen (S) powder to produce layered 2H-WS ₂ and (d) Hydrothermal method for synthesizing WS ₂ in an autoclave at high temperature and pressure.....	36
	Fig. 2.4	Illustrative depiction of 2D material transfer methods by dry and wet transfer techniques: (a) Chemical etching wet transfer (b) Electrochemical bubble transfer (c) Scotch tape dry transfer and (d) Chemical etchant-assisted dry transfer method.....	40
	Fig. 2.5	Illustrative depiction of the traditional Si-based MOSFET and back-gate, top-gate and dual-gated WS ₂ -FET structure.....	42
	Fig. 2.6	The energy band diagram illustrates the Metal-Semiconductor interface for an n-type semiconductor: before and after contact, and the M-S junction can operate in three distinct modes: accumulation, neutral, and depletion.....	45
	Fig. 2.7	Schematic representation of the atomic lattice structure of WS ₂ with a dopant atom: (a) top view of the doped WS ₂ lattice, and (b) side view of the doped WS ₂ , showing the dopant atom positioned on the top layer of WS ₂	47
3	Fig. 3.1	Schematic depiction of the sequential steps of Liquid-phase exfoliation of the WS ₂ nanosheet.....	65
	Fig. 3.2	(a) Raman spectroscopy of the exfoliated 6 hr WS ₂ nanosheets was taken using a 514 nm laser for the surfactant concentration of 2.29 $\mu\text{mol/ml}$, 4.30 $\mu\text{mol/ml}$, 5.16, 6.02 and 6.88, (b) reduce the peak frequency difference (A_{1g} - E_{2g}^1) from 69.7 cm^{-1} for bulk WS ₂ to 65.15 cm^{-1} for 6 hr exfoliated WS ₂ and (c) the difference of Raman spectra after increasing the WS ₂ exfoliation time	

	from 6 hr to 10 hr at a surfactant concentration of 5.16 $\mu\text{mol/ml}$ was measured using a 532 nm laser.....	67
Fig. 3.3	(a) UV-Vis spectra of WS_2 nanosheets at varying exfoliation times (b) correspond UV plot as a function of energy ($h\nu$) (c) after centrifugation at different speeds following 10 hr of exfoliation and (d) Tauc plots of WS_2 nanosheets after 10 hr of exfoliation.....	69
Fig. 3.4	(a) PL Spectra for 6 hr, 8 hr and 10 hr exfoliated WS_2 and (b) Lorentzian functions were used to fit the A and B peaks for 10 hr exfoliated nanosheet.....	70
Fig. 3.5	XRD Spectra of the bulk WS_2 powder and exfoliated WS_2 nanosheets at a sonication time of 6 hr, 8 hr and 10 hr	71
Fig. 3.6	AFM images and corresponding height profiles of WS_2 nanosheets: (a-b) bulk WS_2 flake; exfoliated WS_2 flakes using SDBS at concentrations of (c-d) 2.29 $\mu\text{mol/ml}$; (e-f) 4.30 $\mu\text{mol/ml}$; (g-h) 5.16 $\mu\text{mol/ml}$; and (i-j) wide area AFM image of exfoliated WS_2 flake and corresponding histogram showing the average height distribution.....	72
Fig. 3.7	FESEM image of (a-c) 6 hr, (d-f) 8 hr and (g-i) 10 hr exfoliated WS_2 nanosheets.....	73
Fig. 3.8	(a) TEM image at lower magnification (b) High-resolution TEM image with corresponding SEAD Pattern at 10 nm scale (c) HRTEM image for exfoliated nanosheets and (d) illustrated the defect in the atomic lattice during the exfoliation.....	74
Fig. 3.9	Illustrative representation of the liquid phase exfoliation process of WS_2 nanosheets in an aqueous solvent with SDBS.....	75
4	Fig. 4.1 (a) Schematic representation of the energy band diagram at the metal-semiconductor interface, defining the Φ_B and (b) Resistor network model of the multilayer 2D material with metal contact, illustrating the presence of resistances R_{SB} and R_{IL}	83
	Fig. 4.2 (a) The Band diagram at the contact illustrates interface states, including the tunneling barrier, vdW gap, orbital overlap of the TMD under the metal, and defect states. These factors can modify the SBH and lead to FLP and (b) Metal- WS_2 contact with a high work-function metal typically exhibits a van der Waals gap, whereas an ideal contact can be achieved using a low work-function metal...	85

Fig. 4.3	(a) Schematic representation of a MIS structure, where h-BN serves as the interfacial layer between the metal and the semiconductor, along with the energy band diagram of WS ₂ : (b) Energy band diagram of WS ₂ without the interfacial layer and (c) Energy band diagram of WS ₂ with the interfacial layer.....	87
Fig: 4.4	Schematic illustration of the atomic lattice of (a) pure WS ₂ (b) S vacant WS ₂ and (c) the doping process of a WS ₂ monolayer with an n-type dopant atom.....	88
Fig 4.5	Schematic representation of the molecular doping technique.....	91
Fig. 4.6	DFT calculated energy band diagram and DOS for (a) pure WS ₂ (b) WS ₂ with an O atom and (c) Cl atom occupying a sulfur vacancy site in the WS ₂ supercell.....	93
Fig. 4.7	Illustrates spectroscopic analysis for the Undoped and Cl doped WS ₂ thin-film: (a & b) Raman spectroscopy for 6 hr and 10 hr exfoliated nanosheets, (c & d) PL Spectroscopy analysis.....	95
Fig. 4.8	XRD analysis of the undoped and doped WS ₂ nanosheets with varying the doping time.....	96
Fig. 4.9	(a) and (b) represent the FESEM images for undoped and 24 hr Cl doped WS ₂ nanosheets.....	97
Fig. 4.10	(a) and (b) Represents the EDX spectrum of undoped and Cl-doped WS ₂ nanosheet and (c-f) corresponding colour mapping for W, S, O and Cl atom for doped WS ₂	98
Fig. 4.11	(a) Schematic illustration of two terminal WS ₂ devices (b) displays the I-V characteristics and (c) current measured at different temperature ranges plotted as a function of doping duration (d) R _C extraction using TLM method: R _T vs Channel length (e) Activation energy plots for determination of barrier height for undoped and doped WS ₂ and (f) displays the variation of Φ _B vs Doping time.....	102
Fig. 4.12	Schematic depiction of energy band diagram for metal and semiconductor junction (a) before their physical contact and (b) M-WS ₂ at equilibrium condition for both undoped and doped WS ₂	103

5	Fig. 5.1	Illustrative representation of the various 2D-FET structures. (a) Back-gate FET, where the gate electrode is located beneath the dielectric layer and the channel material. (b) Top-gate FET, where the gate electrode is positioned on top of the channel material with an insulating layer separating them (c) Dual-gated FET, which incorporates both top and back gates.....	113
	Fig. 5.2	Schematic depiction of the sequential steps of the device fabrication using contactless photography process.....	116
	Fig. 5.3	(a) Raman Spectroscopy of the FL-WS ₂ nanosheet before and after lithography-based fabrication (b) spectral fitting with Lorentzian curves for 2LM and E _{2g} ¹ and (c) PL Spectroscopy of the exfoliated WS ₂ nanosheets and (d) Optical microscopic image of the photolithography patterned FL-WS ₂ FET device.....	119
	Fig. 5.4	(a) AFM image of the Fabricated FL-WS ₂ device with <10 nm thick nanosheet and (b) corresponding height profiling of the Metal and WS ₂ after the fabrication of the FET.....	120
	Fig. 5.5	(a) FESEM image of the Fabricated FL-WS ₂ device, (b & c) EDAX spectra of the FL-WS ₂ flake captured from different regions of the nanosheet and (d-e) corresponding colour mapping of the W and S atoms in the WS ₂ flake.....	120
	Fig. 5.6	Schematic depiction of the back gated WS ₂ -FET structure on SiO ₂ /Si substrate.....	121
	Fig. 5.7	Schematic depiction of WS ₂ -FET device structure with a channel length of ~2 μm: (a) Cr/Ag metal contact and (b) Ti/Ag metal contact-based FET, (c) output characteristics (I _{ds} -V _{ds}) of Cr/Ag contact based WS ₂ FET and (d) corresponding energy band diagram of Cr-WS ₂ interfaces (e) output characteristics I _{ds} -V _{ds} of the Ti/Ag contact based WS ₂ -FET(f) energy band diagram of Ti-WS ₂ interfaces.....	123
	Fig. 5.8	Transfer characteristics I _{ds} -V _{gs} of the WS ₂ -FET for (a) Cr/Ag metal contact and (b) Ti/Ag metal contact for channel length of ~2 μm.....	124
	Fig. 5.9	Determination of V _{th} from the I _{ds} -V _{gs} plot of the WS ₂ -FETs and extraction of transconductance from the slope ($g_m = \frac{dI_{ds}}{dV_{gs}}$) of the I _{ds} -V _{gs} plot in linear scale for (a & b) Cr contact-based WS ₂ -FET and (c & d) Ti contact-based WS ₂ -FET.....	126

Fig. 5.10	I_{ds} - V_{ds} and I_{ds} - V_{gs} for the Ti contact based WS_2 -FET for (a & b) 3 μm and (c & d) 4 μm channel length.....	128
Fig. 5.11	(a) Variation of drain current I_{ds} from output characteristics of WS_2 -FET with Ti contact (b) ON current of the FETs are plotted as a function of channel length (c) threshold voltage V_{th} extracted from the I_{ds} - V_{gs} plot (d) calculated field effect mobility μ_{FE} and subthreshold swing SS plotted as a function of channel length.....	129
Fig. 5.12	I_{ds} - V_{ds} and I_{ds} - V_{gs} characteristics of the doped WS_2 -FET for channel length of 2 μm : (a & b) for Cr/Ag and (c & d) Ti/Ag contact.....	130
Fig. 5.13	(a) I_{on} and field-effect mobility μ_{FE} for both undoped and doped WS_2 -based FET and (b) SS for both undoped and doped WS_2 -based FET.....	131
Fig. 5.14	Y-Function ($\frac{I_{ds}}{\sqrt{g_m}}$) plotted as a function of V_{gs} at constant V_{ds} for devices: (a) D1: Cr contact (b) D2: Ti contact and (c) D3- Cr contact with Doped WS_2 and (d) D4: Ti contact with Doped WS_2 -FET and V_{th} is extracted from the x-axis intercept of the linear fit of the characteristics curve.....	133
Fig. 5.15	Comparison of field-effect mobility (extracted from linear extrapolation of I_{ds} - V_{gs} and intrinsic mobility (calculated using the Y-function method) for doped and undoped WS_2 -based FETs. Devices: D1 (Cr contact), D2 (Ti contact), D3 (Cr contact with doping), and D4 (Ti contact with doping).....	134
Fig. 5.16	The path of current flow from metal to WS_2 in the FET device is schematical illustrated.....	135
Fig. 5.17	(a) R_T at different V_{ds} for extraction of series resistance R_{SD} and (b) the distribution of the R_{SD} value plotted against $1/(V_{gs}-V_{th})$ for the extraction of $2R_C$	136
Fig. 5.18	(a) Variation of R_C with n_s for both doped and undoped WS_2 -FETs and (b & c) energy band diagram of Metal- WS_2 interface for undoped and doped WS_2 -based FET.....	137

List of Tables:

Chapter	Table	Title	Page No.
1	1.1	Comparative study of the properties and applications of WS ₂ and MoS ₂	13
2	2.1	Structural properties of WS ₂	32
	2.2	Bandgap comparison of Si and 2D semiconductor materials.....	34
	2.3	Summary of performances of different Top, bottom and dual-gated TMD-FETs.....	44
	2.4	Performance comparison of TMD-FETs with electrical polarity modulation achieved via substitutional atomic doping.....	49
3	3.1	Summary of representative works on LPE of WS ₂ using different exfoliating agents.....	64
	3.2	Experimental Parameters for SDBS-Assisted Exfoliation of WS ₂ Nanosheets.....	65
	3.3	Characteristic of the frequency peak of bulk and exfoliated WS ₂ samples.....	67
4	4.1	Variation of SBH, R _C and Mobility in TMD-based transistor devices with work-function dependent metal contacts or n-type doping.....	89
	4.2	Process summary of molecular doping of WS ₂ using 1,2-dichloroethane.....	92
	4.3	Shift of PL peak with varying doping time.....	96
	4.4	Atomic Percentage of Undoped and Doped WS ₂	99

Nomenclature

Abbreviations:

Si	Silicon
SiO ₂	Silicon Dioxide
MOSFET	Metal Oxide Field-Effect Transistors
M-S	Metal-Semiconductor
FET	Field-Effect Transistors
SOI	Silicon-On-Insulator
1D	One-Dimensional
2D	Two Dimensional
NW	Nanowire
NT	Nanotube
CNT	Carbon Nanotube
CNR	Carbon Nanoribbon
SWNT	Single-Wall Nanotube
MWNT	Multiwall Nanotube
NR	Nanoribbon
NRO	Nanorod
BP	Black Phosphorus
TMD	Transition Metal Dichalcogenide
GAA	Gate-All-Around
Au	Gold
ZnO	Zinc Oxide
TiO ₂	Titanium Dioxide
GaN	Gallium Nitride
vdW	Van-der Waals
CVD	Chemical Vapor Deposition
X	Chalcogen
Mo	Molybdenum
W	Tungsten

S	Sulfur
Se	Selenide
Ti	Titanium
WS ₂	Tungsten Disulfide
MoS ₂	Molybdenum Disulfide
MoSe ₂	Molybdenum Diselenide
WSe ₂	Tungsten Diselenide
MoTe ₂	Molybdenum Ditelluride
PL	Photoluminescence
UV-Vis	UV-Visible
XRD	X-Ray Diffraction
FESEM	Field Emission Scanning Electron Microscopy
AFM	Atomic Force Microscopy
HRTEM	High Resolution Transmission Electron Microscopy
EDX	Energy-Dispersive X-ray
SBH	Schottky Barrier Height
I-V	Current-Voltage
LPE	Liquid-Phase Exfoliation
Cl	Chlorine
DFT	Density Functional Theory
DOS	Density of States
OT	Octahedral
CBM	Conduction Band Minimum
VBM	Valence Band Maximum
SOC	Spin-Orbit Coupling
C	Carbon
TTF	Tetrathiafulvalene
TCNQ	Tetracyanoquinodimethane
HOMO	Highest Occupied Molecular Orbital
LUMO	Lowest Unoccupied Molecular Orbital
NMP	N-Methyl-2-Pyrrolidone
DMF	N-Dimethylformamide

ACE	Acetone
DI	Deionized
EtOH	Ethanol
IPA	Isopropyl Alcohol
PVD	Physical Vapor Deposition
MBE	Molecular Beam Epitaxy
VDWE	Van-der Waals Epitaxy
PLD	Pulsed Laser Deposition
EBE	Electron Beam Evaporation
O ₂	Oxygen
TB-WS ₂	Twisted Bilayer-Tungsten Disulfide
Ar	Argon
PMMA	Poly (Methyl Methacrylate)
K ₂ S ₂ O ₈	Potassium Persulfate
NaOH	Sodium Hydroxide
Na ₂ SO ₄	Sodium Sulfate
PDMS	Polydimethylsiloxane
PET	Poly(Ethylene Terephthalate)
ALD	Atomic Layer Deposition
Al ₂ O ₃	Aluminum Dioxide
HfO ₂	Hafnium Dioxide
OH	Hydroxyl
V	Vanadium
(RhCpCp*) ₂	Pentamethylrhodocene Dimer
P ₂ O ₅	Phosphorous Pentoxide
Na	Sodium
LiF	Lithium fluoride
TEA	Triethylamine
PPh ₃	Triphenylphosphine
AuCl ₃	Gold Chloride
BV	BenzyI Viologen
Li ⁺	lithium-Ion

Cu	Copper
h-BN	Hexagonal Boron Nitride
ITO	Indium Tin Oxide
MeOH	Methanol
$(\text{NH}_4)_2\text{CO}_3$	Ammonium Carbonate
CHP	Cyclohexylpyrrolidone
PEG	Polyethylene Glycol
HMT	Hexamethylenetetramine
SC	Sodium Cholate
CTAB	Cetyltrimethylammonium Bromide
SDBS	Sodium Dodecyl Benzene Sulfonate
FWHM	Full Width Half Maximum
SAED	Selected Area Electron Diffraction
MIGS	Metal-Induced Gap States
FLP	Fermi Level Pinning
Ge	Germanium
MIS	Metal-Insulator-Semiconductor
KI	Potassium Iodide
Fe	Iron
DCE	1,2-Dichloroethane
GUI	Graphical User Interface
QE	QUANTUM-ESPRESSO
RT	Room Temperature
VB	Valence Band
CB	Conduction Band
TLM	Transmission Line Model
EOT	Equivalent Oxide Thickness
FL	Few-Layer
HF	Hydrofluoric Acid
N_2	Nitrogen
Al	Aluminium

Symbols:

Λ	Intermediate point
A_{1g}	out-of-plane
E_{2g}^1	in-plane
N	Nanosheet Thickness
λ_A	A Exciton
A^o	Exciton
A^-	Trion
c	Lattice Constant
d	Interplanar Spacing
E_g	Bandgap
E_F	Fermi level
E_{CNL}	Charge Neutrality
R_{SB}	Schottky Barrier Resistance
R_{IL}	Interlayer Resistance
R_{Ch}	Channel Resistance
R_T	Total Resistance
R_{SD}	Series Resistance
R_{Sh}	Sheet Resistance
ρ_C	Contact Resistivity
L_T	Transfer Length
Φ	Work Function
Φ_S	Semiconductor Work Function
Φ_M	Metal Work Function
χ_s	Electron Affinity
Φ_B	Schottky Barrier
I_0	Saturation Current
k	Boltzmann Constant
T	Temperature
e	Charge of an Electron
A	Contact Area

A^*	Richardson Constant
V_{gs}	Gate-Source Voltages
I_{ds}	Drain Source Current
V_{ds}	Drain Source Voltage
I_{max}	Maximum Current
I_{min}	Minimum Current
I_{on}	On Current
L	Channel Length
W	Channel Width
μ_{FE}	Field Effect Mobility
μ_0	Intrinsic Mobility
g_m	Transconductance
V_{th}	Threshold Voltage
SBH	Schottky Barrier Height
I_{ON}/I_{OFF}	Current ON OFF Ratio
E_{FM}	Metal Fermi Level
E_{FS}	Semiconductor Fermi Level
E_{VAC}	Vacuum Level
R_C	Contact Resistance
n_s	Carrier Concentration
C_{ox}	Oxide Capacitance
C_{it}	Interface-Trap Capacitance
SS	Subthreshold Slope
D_{it}	Interface Trap Density
θ	Mobility Attenuation Coefficient